

PACS numbers: 42.62.Fi; 42.55.Rz; 42.55.Px
DOI: 10.1070/QE2013v043n09ABEH015231

Intracavity laser spectroscopy with a semiconductor disk laser-pumped cw Cr^{2+}:ZnSe laser

V.I. Kozlovsky, Yu.V. Korostelin, O.G. Okhotnikov, Yu.P. Podmar'kov, Ya.K. Skasyrsky, M.P. Frolov, V.A. Akimov

Abstract. **Absorption spectra of the air have been measured near 2.31 μm using intracavity laser spectroscopy with a semiconductor disk laser-pumped cw Cr^{2+}:ZnSe laser. It is shown that, at lasing times of at least 3 ms, the sensitivity of the laser to intracavity absorption increases. This allows one to reach an effective path length of 900 km and enables detection of weak lines with absorption coefficients down to 1×10^{-9} cm^{-1}.**

Keywords: *intracavity laser spectroscopy, Cr^{2+}:ZnSe laser, semiconductor disk laser.*

1. Introduction

II–VI crystals doped with divalent transition metal ions have shown considerable potential as gain media for tunable mid-IR lasers. Lasers based on such crystals have a broad pump absorption band and low lasing threshold, can operate in both continuous and pulsed modes at room temperature, are tunable over a wide spectral range and can conveniently be pumped by many types of lasers and laser diodes. Their broad gain band makes them promising for ultrashort pulse generation. Moreover, they have a homogeneously broadened gain profile, which allows their emission bandwidth to be reduced when necessary, with no significant output power loss. Each material of the type in question has a wide continuous tuning range (~1000 cm^{-1}) and taken together they enable efficient lasing in the spectral range 2–6 μm [1–15].

It seems promising to employ the lasers in question in intracavity laser spectroscopy (ILS) [16] for high-sensitivity detection of weak absorption lines in the mid-IR spectral region. The use of ILS enables the sensitivity of absorption spectroscopy to be improved by many orders of magnitude compared to conventional techniques. This is achieved by placing an absorbing gas in the cavity of a multimode (broadband) laser. During a laser pulse, the laser beam repeatedly passes through the absorbing layer. If the physical path length of the sample cell containing the absorbing gas is tens of centimetres, effective path lengths of tens and hundreds of kilometres can be obtained, which is impossible in conventional absorption spectroscopy. Owing to this, one can detect ultralow impurity concentrations in the air.

There is particular interest in lasers whose spectral range contains strong absorption lines of diverse substances. It is for this reason that there is currently a pronounced tendency for the spectral range of most high-sensitivity laser absorption methods to be extended to the IR, which stems from the quest to reduce the detection limits for gases, many of which have relatively strong IR absorption lines, resulting from vibrational transitions.

ILS employs lasers with a broad emission band, in which the homogeneous width of the gain profile of their active medium is large compared to the width of the absorption line of the gas of interest, placed in the laser cavity. The effective path length is then determined by the path length passed by the light during the lasing time and increases with increasing lasing time. This is, however, only valid below a certain limit, which depends on properties of a particular gain medium. For example, when solid-state lasers were used in ILS, an experimentally observed linear rise in absorption signal was observed for up to 12 ms for a neodymium glass laser [17], up to 4 ms for a $Co^{2+}:MgF_2$ laser [18] and up to 4.5 ms for a $Ti^{3+}:Al_2O_3$ laser [19]. In the case of a vertical-external-cavity surface-emitting semiconductor laser, the signal was reported to increase for no more than 320 μs [20]. At the noise level realised in that study (0.25%), this ensured a detection limit for weak absorption lines of down to 3×10^{-10} cm^{-1}. The best sensitivity (1.2×10^{-11} cm^{-1}) was demonstrated with a dye laser [19], in which the intracavity absorption signal was observed to rise for up to 230 ms.

Lasers based on II–VI crystals doped with transition metal ions were also employed in ILS. In particular, an Fe^{2+}:ZnSe laser was used to measure absorption spectra of methane in the 4.1 μm range with an effective path length of 24 km [21], and Cr^{2+}:ZnSe lasers were successfully used to measure absorption spectra in the 2.5 μm range [22–24]. However, the maximum effective path length obtained to date with these lasers is within 70 km.

This paper addresses the dynamics of the output spectrum of a cw-pumped Cr^{2+}:ZnSe laser with the aim of increasing the effective path length in ILS. In previous ILS studies, Cr^{2+}:ZnSe lasers were optically pumped by pulsed Co:MgF_2 and Er:YAG lasers [22, 23] and a cw fibre laser [24]. In this

V.I. Kozlovsky, Yu.V. Korostelin, Ya.K. Skasyrsky P.N. Lebedev Physics Institute, Russian Academy of Sciences, Leninsky prosp. 53, 119991 Moscow, Russia;
O.G. Okhotnikov Optoelectronics Research Centre, Tampere University of Technology, P.O. Box 692, FIN-33101 Tampere, Finland;
Yu.P. Podmar'kov, M.P. Frolov Moscow Institute of Physics and Technology (State University), Institutskii per. 9, 141700 Dolgoprudnyi, Moscow region, Russia; P.N. Lebedev Physics Institute, Russian Academy of Sciences, Leninsky prosp. 53, 119991 Moscow, Russia; e-mail: frolovmp@x4u.lebedev.ru;
V.A. Akimov Moscow Institute of Physics and Technology (State University), Institutskii per. 9, 141700 Dolgoprudnyi, Moscow region, Russia

Received 16 May 2013; revision received 26 June 2013
Kvantovaya Elektronika **43** (9) 885–889 (2013)
Translated by O.M. Tsarev

study, a semiconductor disk laser (SDL) was used as a pump source [25]. A distinctive feature of SDLs is high output power in combination with high efficiency and excellent beam quality. This makes them potentially attractive for use in ILS and compact device development.

2. Experimental setup and procedure

The gain element of the Cr^{2+}:ZnSe laser was cut from a Cr^{2+}:ZnSe single crystal grown from the vapour phase on a single-crystal seed at temperatures in the range 1100–1150 °C, with concurrent doping by a procedure developed previously for the growth of homogeneous crystals of solid solutions [26, 27]. The advantages of this procedure over other approaches, such as growth from a properly doped melt or vapour growth of undoped crystals followed by solid-state dopant indiffusion through the crystal surface, are high structural perfection and optical homogeneity of the crystals. Owing to this, crystals grown using this procedure offer low internal losses. Mass transport in the vapour phase is ensured by physical transport in helium.

Figure 1 shows a schematic of the experimental setup. The gain element of the Cr^{2+}:ZnSe laser was 2 mm in length and 2×8 mm in cross-sectional dimensions. The Cr^{2+} concentration in the ZnSe crystal was 5×10^{18} cm^{-3}. We used a four-mirror cavity formed by a totally reflecting flat mirror (M1), two intermediate, spherical (R = 100 mm) mirrors (M2 and M3), spaced 100 mm apart, and a flat output mirror (M4). The gain element was placed at the cavity mode waist at the Brewster angle. The laser cavity was not evacuated.

We studied the dynamics of spectral dips produced in the output spectrum of the Cr^{2+}:ZnSe laser by atmospheric water vapour and methane present in its cavity. The centre wavelength of the laser output spectrum was tuned to 2.31 μm. According to Rothman et al. [28], this wavelength corresponds to one of the atmospheric windows, with relatively weak absorption lines of methane and water molecules. This allows laser operation to be investigated with an extremely high sensitivity to weak absorption lines. The output spectrum was tuned using the cavity mirrors, which had appropriate reflection spectra.

The Cr^{2+}:ZnSe crystal was pumped at a small angle to the optical axis of the cavity by a cw SDL with a wavelength of 1.98 μm and output power of up to 2 W. A similar SDL was used previously to pump a Cr^{2+}:CdSe laser [29]. The nearly diffraction-limited SDL beam divergence ensures quality focusing and allows relatively long crystals to be used in the case of longitudinal pumping (the characteristic length of the gain element in lasers based on II–VI crystals doped with divalent transition metal ions is 2–10 mm).

The pump beam was modulated by a mechanical chopper in the form of a rotating disk having 20 holes 9 mm in diameter, whose centres were the same distance apart along a 115-mm-diameter circle. The edges of neighbouring holes were 9 mm apart. The disk was rotated by a DPM-30-N1-05 motor, whose rotation rate could be continuously tuned. Since the pump beam diameter at the output of the semiconductor disk laser was 3 mm, the chopper disk was placed at the focus of the telescope formed by lenses L1 and L2 in order to ensure a sufficient rate of pump pulse rise. The shape of pump and laser pulses was recorded using PD25 photodiodes (IBSG mid-infrared optoelectronics), whose signals were fed to a Tektronix TDS1012B oscilloscope.

The emission spectrum of the Cr^{2+}:ZnSe laser was measured using upconversion. The broadband IR radiation from the Cr^{2+}:ZnSe laser (peak power of 10 mW) was first converted to a shorter wavelength (λ = 0.497 μm) through mixing with a monochromatic (λ = 0.6328 μm) 5-mW He–Ne laser output in a $LiNbO_3$ nonlinear crystal. The He–Ne laser beam (0.6-mm spot diameter on the disk) was modulated by the same disk as the pump beam. The He–Ne laser and pump beams propagated in a horizontal plane and were 115 mm apart. Note that the laser and pump beams passed through two diametrically opposite holes in the disk. Translating the disk vertically, we were able to vary the time delay of He–Ne laser pulses relative to pump pulses and, hence, relative to

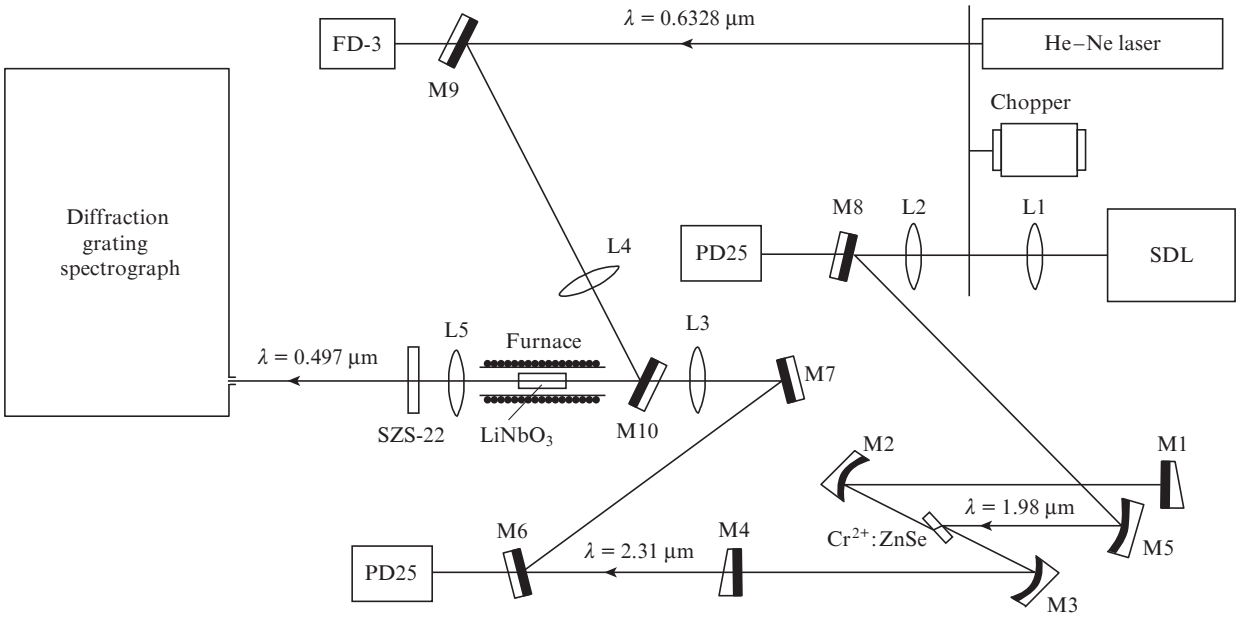

Figure 1. Schematic of the experimental setup: SDL, semiconductor disk laser; Cr^{2+}:ZnSe, gain element of the laser; M1–M10, mirrors; L1–L5, lenses; FD-3 and PD25, photodiodes; $LiNbO_3$, nonlinear crystal.

Cr^{2+}:ZnSe laser pulses. The He–Ne laser beam was sent to an FD-3 photodiode, whose signal was fed to the Tektronix TDS1012B. The diagram in Fig. 2 illustrates the relative position of the Cr^{2+}:ZnSe and He–Ne laser pulses. Only the radiation near the trailing edge of the Cr^{2+}:ZnSe laser pulses, which was mixed with the radiation near the leading edge of the He–Ne laser pulses (grey areas in Fig. 2), was converted to the visible range. The duration of the overlapping parts of the pulses was within 10% of the total pulse duration.

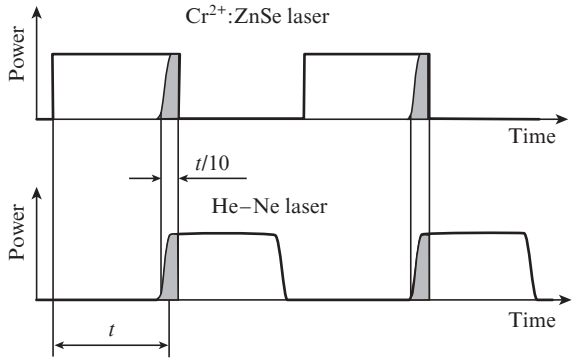

Figure 2. Time diagram illustrating the relative position of Cr^{2+}:ZnSe and He–Ne laser pulses.

The Cr^{2+}:ZnSe and He–Ne laser beams were focused and combined in the lithium niobate crystal using mirrors M6, M7 and M9, lenses L3 and L4 and a dichroic mirror (M10), which had nearly 100% reflectivity at a wavelength of 0.6328 μm and was transparent around 2.31 μm. The $LiNbO_3$ crystal was mounted in a furnace in the form of a Nichrome wire-wound silica tube. To ensure 90° phase matching, the $LiNbO_3$ crystal was heated to a temperature of about 250 °C. The converted radiation was separated out by an SZS-22 (blue-green glass) optical filter and focused by lens L5 onto the entrance slit of a diffraction grating spectrograph (0.06-cm^{-1} resolution) equipped with a computer-interfaced linear CCD array detector. Varying the chopper rotation rate, we were able to tune the lasing time of the Cr^{2+}:ZnSe laser in the range 0.1–3 ms, record the emission spectrum of the Cr^{2+}:ZnSe laser in this time range and follow the time evolution of intracavity absorption spectra.

3. Experimental results and discussion

As an example, Fig. 3 shows measured emission spectra of the Cr^{2+}:ZnSe laser at different lasing times t_l. The signal acquisition time in the measurements was 10 s. The spectra were obtained at a pump power a factor of 1.6 higher than the lasing threshold. The observed absorption lines are due to atmospheric methane and water vapour. Also presented in Fig. 3 are transmission spectra of the air which were obtained by numerical simulation with allowance for previous data [28], the envelope of the laser output spectrum and the measured water vapour partial pressure (4.3 Torr) and measured methane gas concentration (2 ppm) in the laboratory. The line profile in the simulation was assumed to be Lorentzian. The absorbing layer thickness L_{abs} was taken to be equal to the beam path length during the lasing time. In addition, the

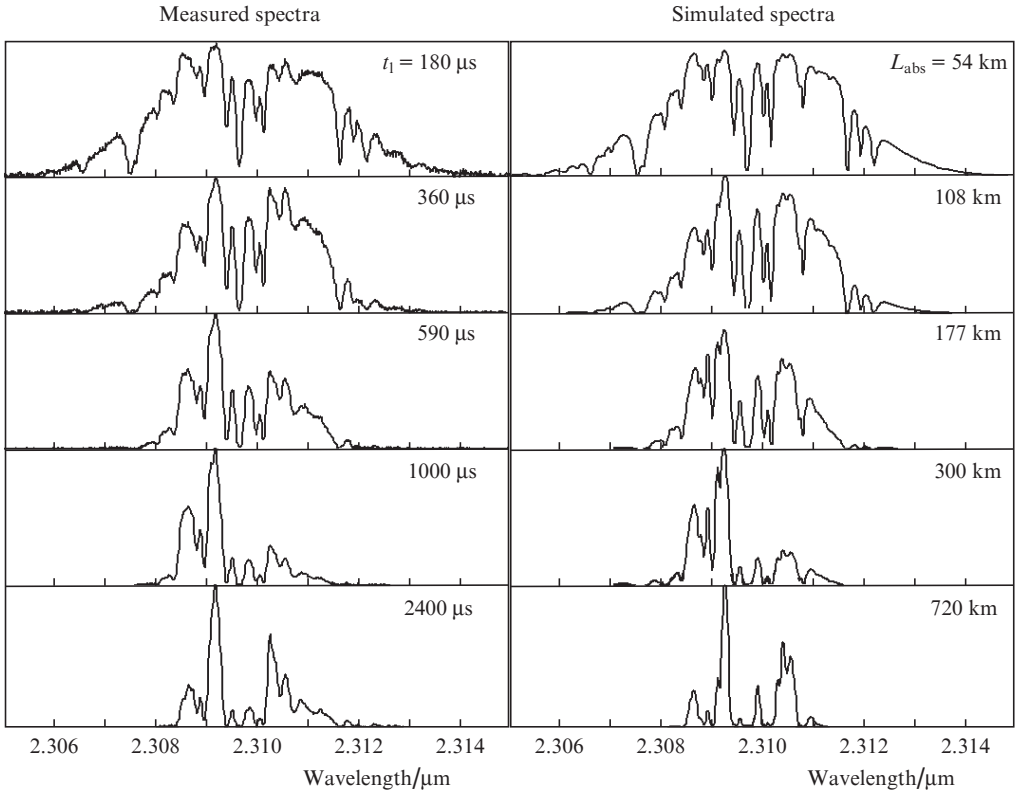

Figure 3. Measured emission spectra of the Cr^{2+}:ZnSe laser with intracavity absorption (atmospheric air) at different lasing times t_l and simulated transmission spectra of the air which were obtained with allowance for the envelope of the laser output spectrum.

instrumental function of the spectrograph was taken into account.

The simulated and measured spectra agree throughout the spectral range studied, except between 2.3104 and 2.3108 μm. According to Rothman et al. [28], the strongest absorption in this range is due to absorption lines of water vapour at frequencies of 4327.52030, 4327.54794, 4327.70028, 4328.16443 and 4328.17301 cm^{-1}. It seems likely that the data presented in Ref. [28] for these lines need to be verified.

For quantitative measurements in ILS, use is made of a modified Bouguer–Lambert–Beer law. When the entire laser cavity is filled with an absorbing substance, this law has the form

$$I(\omega, t) = I_0 \exp[-k(\omega)ct]. \quad (1)$$

Here, $k(\omega)$ is the absorption coefficient at frequency ω; c is the speed of light; $I(\omega, t)$ is the laser light intensity at frequency ω and time t when there is intracavity absorption; and I_0 is the laser light intensity (at frequency ω and time t) when there is no absorption. In practice, I_0 can be found using the envelope of the laser emission spectrum.

Figure 4 shows a semilog plot of the I_0/I ratio against time for the absorption line of methane at 2.309 μm (ω = 4330.9154 cm^{-1}). The data were extracted from the above measured spectra. The plot differs from linear behaviour predicted by (1). This is caused by the following: Under the experimental conditions of this study, absorption lines are highly saturated at long lasing times, i.e. the emitted light intensity is low in the centre of the lines. For this reason, insufficient resolution of the spectral apparatus leads to significant distortion of results. This is supported by the curve in Fig. 4, which was calculated for the line under consideration with allowance for the actual instrumental function of the spectrograph. There is good agreement between the calculated curve and data points.

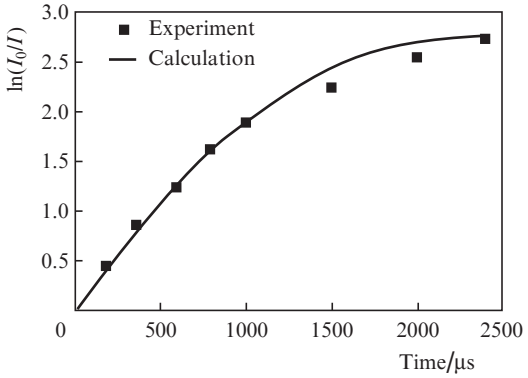

Figure 4. Plot of $\ln(I_0/I)$ against lasing time for the Cr^{2+}:ZnSe laser.

The present results suggest the possibility of creating a Cr^{2+}:ZnSe laser-based ILS spectrometer that would have an effective absorbing layer thickness of ~900 km. Since the noise level allows reliable detection of spectral dips, which amounted to 10%, this ensures sensitivity to lines with absorption coefficients down to $\sim 1 \times 10^{-9}$ cm^{-1}.

Given that strong saturation of absorption lines was observed at laser pulse durations of 3 ms and more, demonstration and investigation of ILS with longer Cr^{2+}:ZnSe laser pulses are possible at lower intracavity concentrations of absorbing molecules, e.g., by enclosing a Cr^{2+}:ZnSe laser in a vacuum chamber.

Thus, it is shown that, in ILS with a cw semiconductor disk laser-pumped Cr^{2+}:ZnSe laser, increasing the lasing time to ~3 ms improves the sensitivity of the method (effective path length of ~900 km). This enables detection of weak absorption lines with absorption coefficients down to $\sim 1 \times 10^{-9}$ cm^{-1}.

Acknowledgements. This work was supported by the RF Ministry of Education and Science (Agreement No. 8519).

References

1. DeLoach L.D., Page R.H., Wilke G.D., Payne S.A., Krupke W.F. *IEEE J.Quantum Electron.*, **32**, 885 (1996).
2. Page R.H., Schaffers K.I., DeLoach L.D., Wilke G.D., Patel F.D., Tassano J.B., Payne S.A., Krupke W.F., Chen K.-T., Burger A. *IEEE J.Quantum.Electron.*, **33**, 609 (1997).
3. Sorokina I.T. *Opt. Mater.*, **26**, 395 (2004).
4. Demirbas U., Sennaroglu A. *Opt. Lett.*, **31**, 2293 (2006).
5. Sorokina I.T., Sorokin E., Mirov S., Fedorov V., Badikov V.V., Panyutin V., Schaffers K.I. *Opt. Lett.*, **27**, 1040 (2002).
6. Seo J.T., Hömmerich U., Trivedi S.B., Chen R.J., Kutcher S. *Opt. Commun.*, **153**, 267 (1998).
7. Trivedi S.B., Kutcher S.W., Wang C.C., Jagannathan G.V., Hömmerich U., Bluiett A., Turner M., Seo J.T., Schepler K.L., Schumm B., Boyd P.R., Green G. *J. Electron. Mater.*, **30**, 728 (2001).
8. Bluiett A., Hömmerich U., Shah R.T., Trivedi S.B., Kutcher S.W., Wang C.C. *J. Electron. Mater.*, **31**, 806 (2002).
9. McKay J., Schepler K.L., Catella G.C. *Opt. Lett.*, **24**, 1575 (1999).
10. McKay J., Roh W.B., Schepler K.L. *OSA Techn. Digest on Advanced Solid-State Lasers*, Paper WA7 (2002).
11. Adams J.J., Bibeau C., Page R.H., Krol D.M., Furu L.H., Payne S.A. *Opt. Lett.*, **24**, 1720 (1999).
12. Voronov A.A., Kozlovsky V.I., Korostelin Yu.V., Landman A.I., Podmar'kov Yu.P., Frolov M.P. *Kvantovaya Elektron.*, **35**, 809 (2005) [*Quantum Electron.*, **35**, 809 (2005)].
13. Akimov V.A., Voronov A.A., Kozlovsky V.I., Korostelin Yu.V., Landman A.I., Podmar'kov Yu.P., Frolov M.P. *Kvantovaya Elektron.*, **36**, 299 (2006) [*Quantum Electron.*, **36**, 299 (2006)].
14. Fedorov V.V., Mirov S.B., Gallian A., Badikov V.V., Frolov M.P., Korostelin Yu.V., Kozlovsky V.I., Landman A.I., Podmar'kov Yu.P., et al. *IEEE J. Quantum Electron.*, **42**, 907 (2006).
15. Mislavskii V.V., Frolov M.P., Korostelin Yu.V., Kozlovsky V.I., Landman A.I., Podmar'kov Yu.P., Skasyrsky Ya.K. *Techn. Program 14-th Intern. Conf. Laser Optics 'LO-2010'* (St. Petersburg, Russia, 2010) p. 60, WeR1-p18.
16. Pakhomycheva L.A., Sviridenkov E.A., Suchkov A.F., Titova L.V., Churilov S.S. *Pis'ma Zh. Eksp. Teor. Fiz.*, **12**, 60 (1970).
17. Baev V.M., Dubov V.P., Sviridenkov E.A. *Kvantovaya Elektron.*, **12**, 2490 (1985) [*Sov. J. Quantum Electron.*, **15**, 1648 (1985)].
18. Frolov M.P., Khan-Magometova S.D., Pazyuk V.S., Podmar'kov Yu.P., Raspopov N.A., Baev V.M. *Proc. SPIE Int. Soc. Opt. Eng.*, **5149**, 155 (2003).
19. Baev V.M., Latz T., Toschek P.E. *Appl. Phys. B.*, **69**, 171 (1999).
20. Garnache A., Kachanov A.A., Stoeckel F., Planel R. *Opt. Lett.*, **24**, 826 (1999).
21. Akimov V.A., Voronov A.A., Kozlovsky V.I., Korostelin Yu.V., Landman A.I., Podmar'kov Yu.P., Frolov M.P. *Kvantovaya Elektron.*, **37**, 1071 (2007) [*Quantum Electron.*, **37**, 1071 (2007)].
22. Akimov V.A., Kozlovsky V.I., Korostelin Yu.V., Landman A.I., Podmar'kov Yu.P., Frolov M.P. *Kvantovaya Elektron.*, **34**, 185 (2004) [*Quantum Electron.*, **34**, 185 (2004)].
23. Akimov V.A., Kozlovsky V.I., Korostelin Yu.V., Landman A.I., Podmar'kov Yu.P., Frolov M.P. *Kvantovaya Elektron.*, **35**, 425 (2005) [*Quantum Electron.*, **35**, 425 (2005)].

24. Girard V., Farreng R., Sorokin E., Sorokina I.T., Guelachvili G., Picque N. *Chem. Phys. Lett.*, **419**, 584 (2005).
25. Okhotnikov O.G. (ed.). *Semiconductor Disk Lasers, Physics and Technology* (Weinheim: Wiley-VCH, 2010).
26. Korostelin Yu.V., Kozlovsky V.I., Nasibov A.S., Shapkin P.V. *J. Cryst. Growth*, **159**, 181 (1996).
27. Korostelin Yu.V., Kozlovsky V.I. *J. Alloys Compd*, **371**, 25 (2004).
28. Rothman L.S., Gordon I.E., Barbe A., et al. *J. Quant. Spectrosc. Radiat. Transfer*, **110**, 533 (2009).
29. Kozlovsky V.I., Korostelin Yu.V., Okhotnikov O.G., Podmar'kov Yu.P., Popov Yu.M., Rautiainen J., Skasyrsky Ya.K., Frolov M.P. *Kratk. Soobshch. Fiz.*, **6**, 30 (2012).